Int. J. Electrochem. Sci., 10 **(2015)** 7371 - 7379

International Journal of
ELECTROCHEMICAL
SCIENCE
www.electrochemsci.org

Hydrothermal Synthesis of Well-dispersed $LiMn_{0.7}Fe_{0.3}PO_4$/C Nanocrystalline Cathodes for Lithium-ion Batteries

Jiangang Li[1,], Pengxiang Zhao[1], Wanlu Duan[3], Li Wang[2,4], Jianjun Li[2,3] and Xiangming He[2,4,*]*

[1] Beijing Institute of Petrochemical Technology, Beijing 102617, China
[2] Institute of Nuclear & New Energy Technology, Tsinghua University, Beijing 100084, China
[3] Huadong Institute of Lithium Ion Battery, Zhangjiagang, Jiangsu 215600, China
[4] State Key Laboratory of Automotive Safety and Energy, Tsinghua University, Beijing 100084
[*]E-mail: hexm@tsinghua.edu.cn; lijiangang@bipt.edu.cn

Received: 2 June 2015 / *Accepted:* 29 June 2015 / *Published:* 28 July 2015

In this work, $LiMn_{0.7}Fe_{0.3}PO_4$/C composite cathode materials were prepared by hydrothermal process followed by carbon-coating. The influence of temperature and the added surfactant CTAB in the hydrothermal process on the structure and electrochemical performance was investigated. The results show that suitable amount of CTAB can reduce the crystal particle growth and improve the particle dispersion, while the particles crystallinity is noticeable affected by the hydrothermal temperature. The sample with higher crystallinity exhibits smaller charge transfer resistance and higher Li^+ diffusion coefficient, and then better electrochemical performance. Well-dispersed $LiMn_{0.7}Fe_{0.3}PO_4$/C nanocrystalline particles can be successfully prepared hydrothermally at 180 ^oC with adding of 0.075 g mL^{-1} CTAB, and present high capacity and excellent rate capability. Its capacity reaches 156.3 mAh g^{-1} at 0.2C, and still remains 132.3 mAh g^{-1} even at 5C.

Keywords: Li-ion batteries; Hydrothermal; Lithium manganese iron phosphate; Carbon-coating

1. INTRODUCTION

Lithium-ion batteries (LIB) have been used as the promising power for EV and HEV due to high energy density and long life [1]. At present, one of the widely used cathode materials in such commercialized LIBs is olivine $LiFePO_4$, which is high safety, low cost, high theoretical capacity (170 mAh g^{-1}) and excellent cycling performance [2]. However, the intrinsically low energy density of $LiFePO_4$ due to low voltage plateau (~3.5V) limits its application. Compared with $LiFePO_4$, olivine $LiMnPO_4$ presents the same theoretical capacity, but higher voltage plateau (~4.1V). Therefore, olivine $LiMnPO_4$ have been investigated thoroughly by many research groups and developed as one of the

most promising next generation cathode materials for EV or HEV used LIB's in recent years [1,3]. Owing to its poorer electronic conductivity than $LiFePO_4$, the recent researches on $LiMnPO_4$ have focused mainly on improving its electrochemical properties by the following modification methods: 1) doping by cation such as Fe, Mg, Zn, Zr, Co, Cr, Ti etc. [4-11]; 2) surface coating by good conduct material such as carbon, reduced grapheme oxide etc. [12-15]; 3) particle size reduction to decrease solid-state Li diffusion path [12,16,17]. As shown in literatures, carbon-coated $LiMn_{1-x}Fe_xPO_4$ (x=0.2~0.5) nano-particles exhibited higher rate capability and large capacity than $LiMnPO_4$.

Carbon-coated $LiMn_{1-x}Fe_xPO_4$ has been reported to be prepared by some methods including solid-state reaction [4-6,17], sol-gel [18,19], hydrothermal reaction [13,15,20-23], solvothermal reaction [24,25], spray-pyrolysis [26], rheological phase reaction [27], electrospinning [28] etc.. Compared with other methods, hydrothermal and solvothermal process has lots of advantages such as phase purity, high crystallinity and narrow particle-size distributions. Researchers have spent more time on hydrothermal and solvothermal process to prepare nano-$LiMn_{1-x}Fe_xPO_4$/C, however, the performance of as-prepared materials still needs to be improved further, and two main problems still require to be solved urgently. One is heavy agglomeration of nano-$LiMn_{1-x}Fe_xPO_4$/C particles, which may lead to decrease of interface area between nano-$LiMn_{1-x}Fe_xPO_4$/C particles and electrolyte, and then increase charge transfer resistance and deteriorate its electrochemical properties [20,23,29]. Another is its poor coating uniformity [15] and conductivity of carbon [22].

In this paper, well-dispersed $LiMn_{0.7}Fe_{0.3}PO_4$/C nanocrystalline particles were synthesized by hydrothermal reaction, followed by carbon coating. In order to improve the dispersion of $LiMn_{0.7}Fe_{0.3}PO_4$/C particles, surfactant hexadecyltrimethylammonium bromide (CTAB) was added in the hydrothermal process. The effects of hydrothermal temperature, surfactant CTAB content on the structural and electrochemical properties of $LiMn_{0.7}Fe_{0.3}PO_4$/C were investigated. Well-dispersed $LiMn_{0.7}Fe_{0.3}PO_4$/C nanocrystalline particles prepared under the optimized conditions exhibited high discharge capacity and good rate capability.

2. EXPERIMENTAL

$LiMn_{0.7}Fe_{0.3}PO_4$ was synthesized by a hydrothermal route from starting materials $LiOH{\cdot}H_2O$, $MnSO_4{\cdot}H_2O$, $FeSO_4{\cdot}7H_2O$, H_3PO_4 in a molar ratio of 1:0.7:0.3:3. Firstly, the solution of transition metal salts ($MnSO_4{\cdot}H_2O$ + $FeSO_4{\cdot}7H_2O$) was slowly dripped into the $LiOH{\cdot}H_2O$, H_3PO_4 and hexadecyltrimethylammonium bromide (CTAB) mixture solution. The concentration of transition metal ions was 0.25 mol L^{-1}, and the CTAB content was 0 g m L^{-1} ~ 0.2 g mL^{-1}. The mixture was stirred vigorous for 10 min, and then poured into a 50 mL Teflon vessel, the Teflon vessel then sealed in a stainless-steel autoclave. Then it was put into a furnace, and then heated at 140 ^oC ~ 180 ^oC for 16 h. After naturally cooling to room temperature, the $LiMn_{0.7}Fe_{0.3}PO_4$ powder was filtered, washed with water and ethanol for several times, and then dried at 80 ^oC in vacuum. Finally, carbon coated $LiMn_{0.7}Fe_{0.3}PO_4$ was obtained by sintering of the mixture of the hydrothermal product with 13 wt.% glucose at 650 ^oC for 10 h under argon atmosphere.

The structure of $LiMn_{0.7}Fe_{0.3}PO_4/C$ powders was characterized by using XRD-7000 X-ray Diffractometer. Morphologies of as-prepared samples were taken from a Philips Quanta-400 field emission scanning electron microscope (SEM). The amount of carbon coated on the particles was analyzed using thermogravimetric analysis (TGA, Beijing Boyuan STA-T7).

CR2032 coin cells were used to characterize the electrochemical performance of as-prepared samples. The cell consisted of a cathode with the composition of 86 wt.% $LiMn_{0.7}Fe_{0.3}PO_4/C$ powders, 8 wt.% Super P carbon black, and 6 wt.% poly(vinylidenefluoride), and a lithium metal anode separated by a Celguard 2400 microporous film. The cathode electrodes were featured with 0.8 cm in diameter and an active area of 0.50 cm^2 respectively. The mass of active material in each cathode was about 5 mg. The electrolyte was 1 mol L^{-1} $LiPF_6$ /EC+DEC+DMC (1:1:1 by volume). The cells were assembled in an Etelux-Lab2000 glove box filled with pure argon. The charge-discharge tests were galvanostatically performed on LAND cell test system over 2.5 V ~ 4.6 V. AC-impedance measurements were performed using a Zahner Elektrik IM6ex impedance analyzer over the frequency range from 100 KHz to 10 mHz with the amplitude of 5 mV.

3. RESULTS AND DISCUSSION

TGA results show that all $LiMn_{0.7}Fe_{0.3}PO_4/C$ samples have almost same carbon content, ~3.2 wt.%. It can be ascribed to the same carbon-coating process after hydrothermally synthesis of $LiMn_{0.7}Fe_{0.3}PO_4$.

Surfacant such as citric acid, CTAB and P123 has been used to control the particle dispersion, size and shape of $LiMnPO_4$ [12] and $LiMn_{1-x}Fe_xPO_4$ [22]. Well-dispersed rod-shape nano-particles can be prepared by CTAB-assisted hydrothermal method. However, the influence of the added CTAB content was unclear. Therefore, the influence of CTAB content on the structure and charge-discharge properties of $LiMn_{0.7}Fe_{0.3}PO_4/C$ was investigated firstly in this work. All samples were hydrothermally synthesized at 180 ^oC. As shown in Fig.1, the added CTAB amounts exert obvious influence on the appearance of particles. For the sample with no added CTAB in hydrothermal process, rod-shape and spindle-shape crystal particles with large size are mixed and agglomerated heavily. Well-dispersed rod-shape crystal particles with reduced particle size can be observed for the sample with adding of 0.075 g mL^{-1} and 0.150 g mL^{-1} CTAB. The particles appearance is very similar to that reported in literatures [12,22]. That indicates that CATB plays important role as dispersant and soft template. With an increase of CTAB content to 0.225 g mL^{-1}, the crystal particle size is further reduced, however, crystal particles dispersion is restrained due to the fact that more crystal particles are close parallel-piled and easily agglomerated.

Fig. 2 shows the XRD patterns and the 5^{th} charge-discharge curves at 0.2C for $LiMn_{0.7}Fe_{0.3}PO_4/C$ prepared with adding different amount of CTAB. All diffraction peaks of as-prepared samples can be indexed on the basis of the structure of orthorhombic *Pnma* olivine phase (JCPDS card PDF 33-0804).

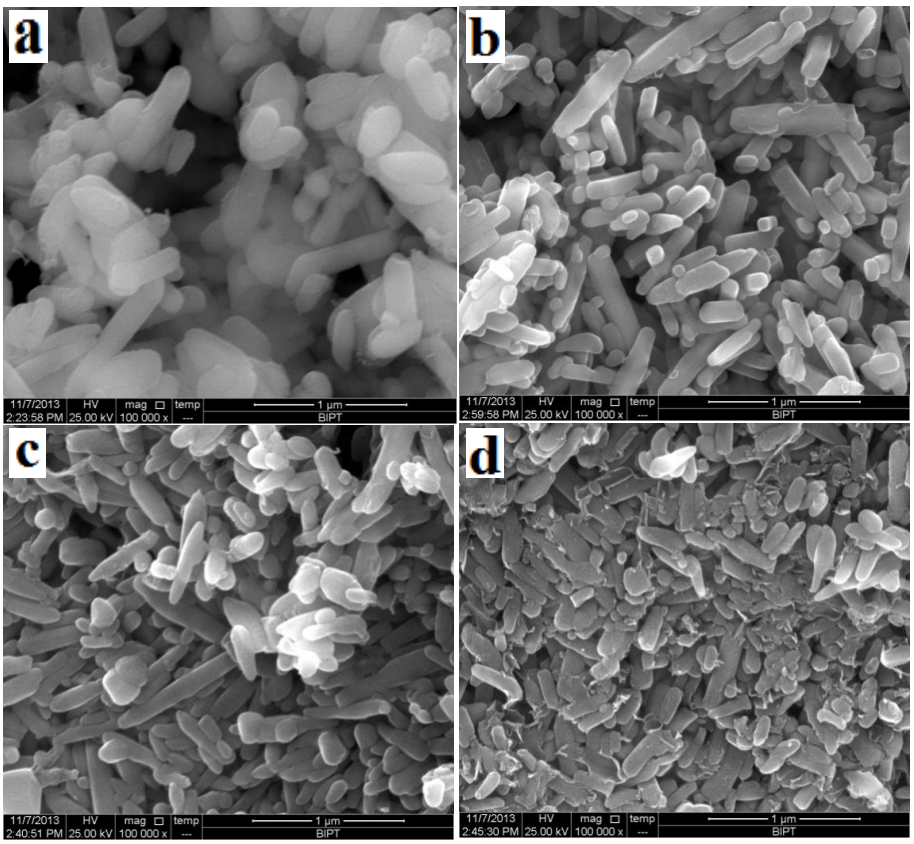

Figure 1. SEM patterns of $LiMn_{0.7}Fe_{0.3}PO_4/C$ prepared by adding different amount of CTAB. (a: 0 g mL^{-1}, b: 0.075 g mL^{-1}, c: 0.150 g mL^{-1}, d: 0.225 g mL^{-1})

The reduction of peak intensity in XRD patterns can be observed for the samples with adding of CTAB, indicating that crystal particles size is decreased. It is consistent with the results shown in Figure 1. The charge-discharge test reveals that all samples exhibit two charge/discharge plateaus around 4.0 V and 3.5 V vs. Li/Li^+ corresponding to the redox couples Mn^{2+}/Mn^{3+} and Fe^{2+}/Fe^{3+}, respectively.

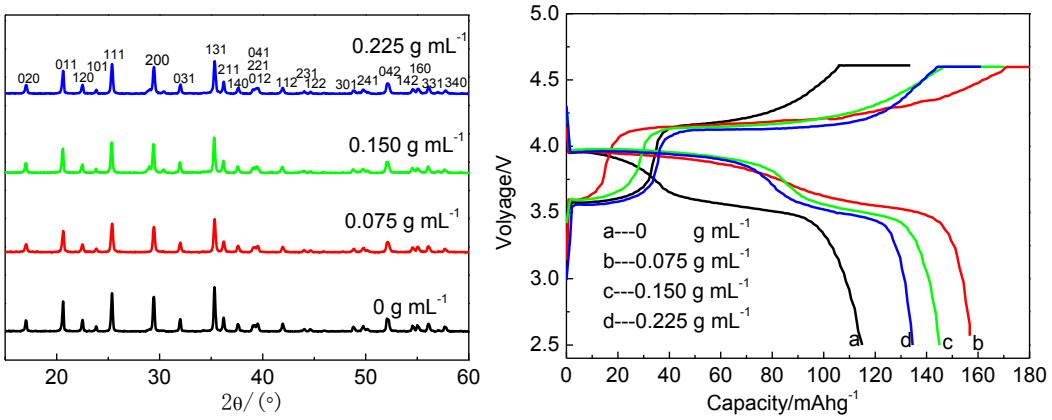

Figure 2. XRD patterns (left) and the 5th charge-discharge curves (right) of $LiMn_{0.7}Fe_{0.3}PO_4/C$ prepared by adding different amount of CTAB

The 0.2C discharge capacity is 114.8 mAh g^{-1}, 157.6 mAh g^{-1}, 145.0 mAh g^{-1} and 134.6 mAh g^{-1} for the sample with adding of 0 g mL^{-1}, 0.075 g mL^{-1}, 0.150 g mL^{-1} and 0.225 g mL^{-1} CATB, respectively. The sample with adding of 0.075 g mL^{-1} CTAB presents the highest capacity, which can be attributed to its good nano-particles dispersion.

Next, the influence of hydrothermal temperature on the structural and electrochemical properties of $LiMn_{0.7}Fe_{0.3}PO_4/C$ was investigated. Based on above research results, the added CTAB amount in the hydrothermal synthesis process of $LiMn_{0.7}Fe_{0.3}PO_4$ was chose to be 0.075 g mL^{-1}. Fig.3 shows the XRD patterns and the 5th charge-discharge curves at 0.2C for $LiMn_{0.7}Fe_{0.3}PO_4/C$ prepared at different hydrothermal temperature. All diffraction peaks of as-prepared samples in XRD patterns are strong and can also be indexed on the basis of the structure of orthorhombic *Pnma* olivine phase, conforming that well-crystalline pure olivine phase samples were prepared. The intensity of peaks increases gradually with a rising of hydrothermal temperature from 140 ^{o}C to 180 ^{o}C, indicating that the crystallinity of as-prepared $LiMn_{0.7}Fe_{0.3}PO_4/C$ particles is improved. However, it is unclear why the crystallinity of as-prepared sample decreases again when the hydrothermal temperature is elevated to 200 ^{o}C.

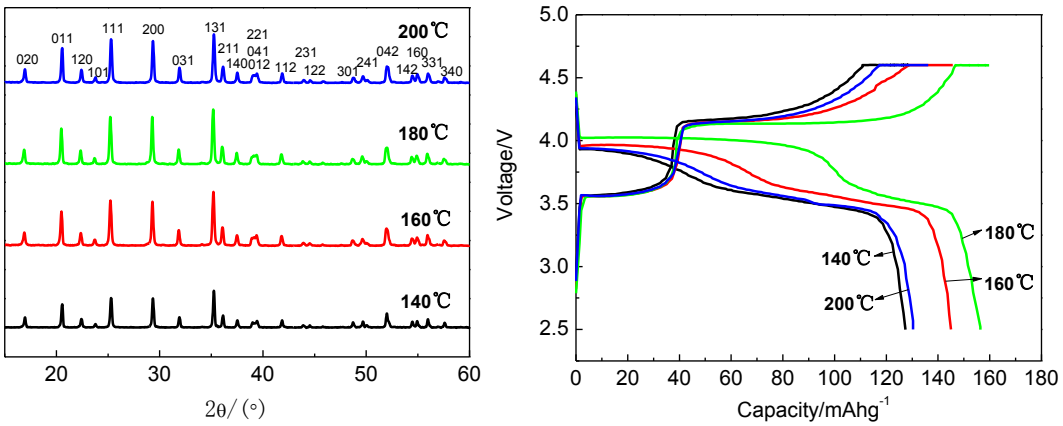

Figure 3. XRD patterns (left) and the 5th charge-discharge curves (right) of $LiMn_{0.7}Fe_{0.3}PO_4/C$ prepared at different hydrothermal temperature

As shown in the 5th charge-discharge curves at 0.2C for $LiMn_{0.7}Fe_{0.3}PO_4/C$ prepared at different hydrothermal temperature, with a rising of hydrothermal temperature from 140 ^{o}C to 180 ^{o}C, the discharge capacity of as-prepared sample increase from 127.39 mAh g^{-1} to 156.35 mAh g^{-1}. However, the capacity for sample synthesized hydrothermally at 200 ^{o}C decrease to 130.32 mAh g^{-1}. Because all samples have same carbon content and similar particle dispersion (Fig.4), the discharge capacity mainly depends on the crystallinity and particle size. Smaller particle size can shorten the Li^+ diffusion path, and better crystallinity can provide higher Li^+ diffusion coefficient D_{Li^+}, therefore, high crystallinity and small particle size are beneficial for the electrochemical performance of $LiMn_{0.7}Fe_{0.3}PO_4/C$. As shown in Fig.4, the sample prepared at 180 ^{o}C has the largest particle size, but presents the highest capacity. In contrast, the capacity variation tendency is in good consistent with the crystallinity varation tendency. It can be deduced that the effect of hydrothermal temperature on the

electrochemical properties of samples is close related to the crystallinity. As far as our knowledge, the related mechanism about influence of hydrothermal temperature on the electrochemical behavior have only been reported by Fang [30] for $LiMnPO_4$, who found that the extent of Mn^{2+} disorder on the Li^+ sites is affected the reaction temperature, which places a strong influence on the lithium ion diffusion and electrochemical activity. If so, the crystallinity may be related to the extent of Mn^{2+} of Fe^{2+} disorder on the Li^+ sites. Further work in this area needs more experimental and theoretical investigations in future.

.

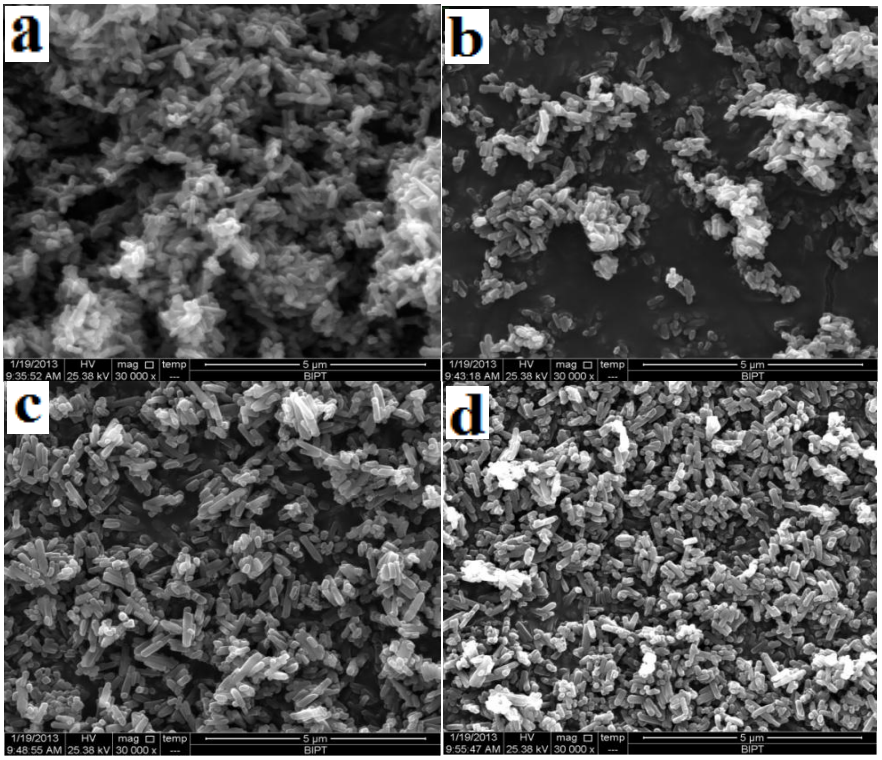

Figure 4. SEM patterns of $LiMn_{0.7}Fe_{0.3}PO_4/C$ prepared at different hydrothermal temperature

In order to further verify the influence of hydrothermal temperature on samples, AC-impedance analysis was carried out, and the results are shown in Fig.5. The spectra of all samples have similar profiles which are composed of a semicircle in the high-to-medium frequency region and an inclined line in the low frequency region. The semicircle is approximately related to the charge transfer process, and the inclined line is associated with the Li^+ diffusion. For sample prepared at 140 ^oC, 160 ^oC, 180 ^oC and 200 ^oC, the charge transfer resistance R_{ct} are simulated to be 162.8 Ω, 137.3 Ω, 65.8 Ω and 149.5 Ω respectively, and the Li^+ diffusion coefficient D_{Li}^+ are calculated to be 3.26×10^{-16} cm^2 s^{-1}, 3.97×10^{-16} cm^2 s^{-1}, 1.23×10^{-15} cm^2 s^{-1} and 3.32×10^{-16} cm^2 s^{-1} respectively based on the low frequency line data [31]. With an increase of hydrothermal temperature from 140 ^oC to 180 ^oC, as-prepared samples show a decreased charge transfer resistance R_{ct} and an elevated Li^+ diffusion coefficient D_{Li}^+, which agrees well with an improved crystallinity and an increased capacity shown in Fig.3. Consistent with decrease of capacity for the sample synthesized at 200 ^oC, the R_{ct} value increases and the Li^+ diffusion coefficient D_{Li}^+ decreases again. Based on the results, it can be speculated that hydrothermal

temperature exerts remarkable influence on the crystallinity and the extent of Mn^{2+} of Fe^{2+} disorder on the Li^+ sites, thus affects the electrochemical performance. The sample prepared at 180 ^oC exhibits the best crystallinity, leading to the smallest charge transfer resistance R_{ct}, the highest Li^+ diffusion coefficient D_{Li}^+ and discharge capacity.

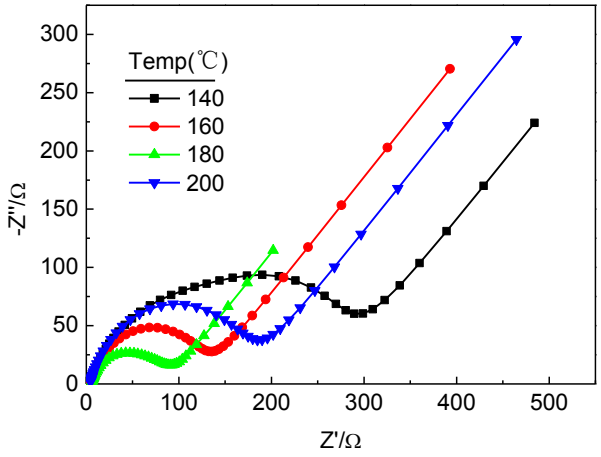

Figure 5. EIS patterns of $LiMn_{0.7}Fe_{0.3}PO_4/C$ prepared at different hydrothermal temperature

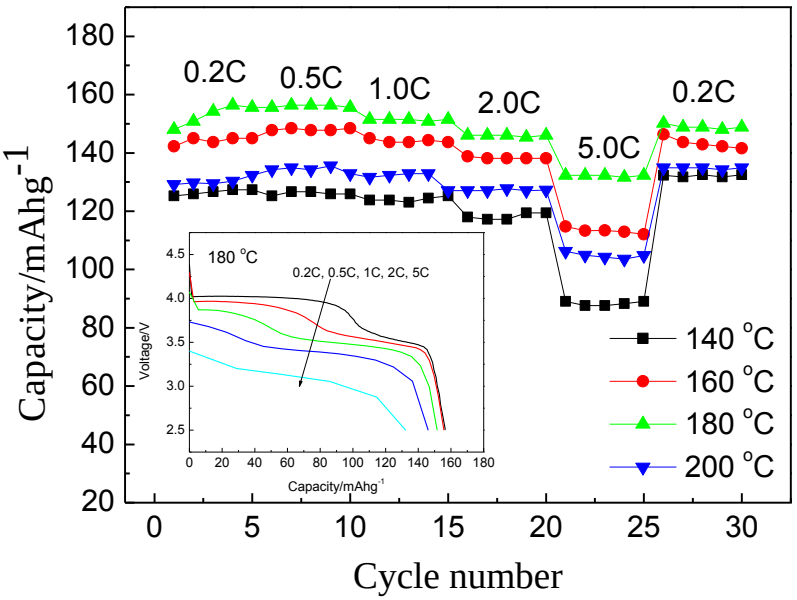

Figure 6. Rate performance of $LiMn_{0.7}Fe_{0.3}PO_4/C$ prepared at different hydrothermal temperature

The rate performance of $LiMn_{0.7}Fe_{0.3}PO_4/C$ prepared at different hydrothermal temperature was also investigated. As shown in Fig.6, the sample prepared at 180 ^oC not only shows the highest capacity, but also exhibits the best rate capability and cycling stability. The discharge capacity reaches 156.3 mAh g^{-1} at 0.2C, 151.5 mAh g^{-1} at 1C, 146.1 mAh g^{-1} at 2C and 132.3 mAh g^{-1} at 5C. Its 0.2C capacity retention after 30 cycles remains 96.1%. It can also be seen from the discharge curves in Fig.6 that at higher discharge rate, the voltage plateau corresponding to the redox couples Mn^{2+}/Mn^{3+}

become shorter, and the voltage plateau corresponding to the redox couples Fe^{2+}/Fe^{3+} become longer, which leads to a capacity maintenance at high rate. It can be attributed to the fact that the reaction of redox couples Mn^{2+}/Mn^{3+} is accelerated by the nucleation enhancer of Fe-doping [32]. Fe-doping combined with carbon coating make great contribution to the improvement of rate capability of $LiMnPO_4$.

4. CONCLUSION

Well-dispersed $LiMn_{0.7}Fe_{0.3}PO_4/C$ nanocrystalline cathode materials were successfully prepared by hydrothermal process followed by carbon-coating. In the hydrothermal process, the added surfactant CTAB exerts no influence on the structure, but can reduce the crystal particle growth and improve the particle dispersion of as-prepared samples. The hydrothermal temperature presents remarkable impact on the crystallinity. The sample with higher crystallinity exhibits smaller charge transfer resistance and higher Li^+ diffusion coefficient, and then better electrochemical performance. The sample synthesized hydrothermally at 180 ^oC with adding of 0.075 g mL^{-1} CTAB displays high capacity and excellent rate capability. Its capacity reaches 156.3 mAh g^{-1} at 0.2C, and still remains 132.3 mAh g^{-1} at 5C, implying that it is a very promising cathode material for EV Li-ion batteries.

ACKNOWLEDGEMENTS

This work is supported by BIPT-supported Project of Outstanding Professors and Management Experts (BIPT-POPME-2013) , the MOST (Grant No. 2013CB934000, No. 2011CB935902, No. 2014DFG71590, No. 2013AA050903, No. 2011AA11A257 and No. 2011AA11A254), the Tsinghua University Initiative Scientific Research Program (Grant No. 2011THZ08139, No. 2011THZ01004 and No. 2012THZ08129), Beijing Municipal Program (Grant No. YETP0157, No. Z131100003413002 and No. Z131100003413001) and State Key Laboratory of Automotive Safety and Energy (No. ZZ2012-011), Suzhou (Wujiang) Automotive Research Institute (Project No.2012WJ-A-01).

References

1. S. J. Gerssen-Gondelach, A. P.C. Faaij, *J. Power Sources,* 212 (2012) 111.
2. Y. Zhang, Q.-Y. Huo, P.-P. Du, L.-Zh. Wang, A.-Q. Zhang, Y.-H. Song, Y. Lv, G.-Y. Li, *Synthetic Metals,* 162 (2012) 1315.
3. B. Xu, D. Qian, Z. Wang, Y. S. Meng, *Mater. Sci. Eng., R* 73 (2012) 51.
4. J. Hong, F. Wang, X. Wang, J. Graetz, *J. Power Sources,* 196 (2011) 3659.
5. Y. Mi, P. Gao, W. Liu, W. Zhang, H. Zhou， *J. Power Sources,* 267 (2014) 459.
6. S.-Y. Yan, Ch.-Y. Wang, R.-M. Gu, S. Sun, M.-W. Li, *J. Alloys Comp.,* 628 (2015) 471.
7. T. Shiratsuchi, S. Okada, T. Doi, J. Yamaki, *Electrochimica Acta,* 54 (2009) 3145.
8. I. Taniguchi, T. N. L. Doan, B. Shao, *Electrochimica Acta,* 56 (2011) 7680.
9. H. Fang , H. Yi, C. Hu, B.Yang , Y. Yao, W. Ma,Y. Dai, *Electrochimica Acta,* 71 (2012) 266.
10. Y. Gan, C. Chen, J. Liu, P. Bian, H. Hao, A. Yu, *J. Alloys Comp.,* 620 (2015) 350.
11. J. Liu, X. Liu, T. Huang, A. Yu, *Int. J. Electrochem. Sci.,* 7 (2012) 9859.
12. H.-C. Dinh, S. Mho, Y. Kang, I.-H. Yeo, *J. Power Sources,* 244 (2013) 189.
13. Z.-Q. Huo, Y.-T. Cui, D. Wang, Y. Dong, L. Chen, *J. Power Sources,* 245 (2014) 331.

14. H. Fang, E. Dai, K. Yang, B. Yang, Y. Yao, W. Ma, Y. Dai, *Int. J. Electrochem. Sci*., 7 (2012) 11827.
15. C. Xu, L. Li, F. Qiu, C. An, Y. Xu, Y. Wang, Y. Wang, L. Jiao, H. Yuan, *J. Ener. Chem.*, 23(2014)397.
16. H. Ji, G. Yang, H. Ni, S. Roy, J. Pinto, X. Jiang, *Electrochimica Acta*, 56 (2011) 3093.
17. Q.-Q. Zou, G.-N. Zhu, Y.-Y. Xia, *J. Power Sources*, 206 (2012) 222.
18. J. Yao, S. Bewlay, K. Konstantionv, V.A. Drozd, R.S. Liu,X.L. Wang, H.K. Liu, G.X. Wang, *J. Alloys Comp.*, 425 (2006) 362.
19. T. T. D. Nguyen, L. Dimesso, G. Cherkashinin, J. C. Jaud, S. Lauterbach, R. Hausbrand, W. Jaegermann, *Ionics*, 19 (2013) 1229.
20. K. Saravanan, J.J. Vittal, M.V. Reddy, B.V.R. Chowdari, P. Balaya, *J. Solid State Electrochem.*, 14 (2010) 1755.
21. K. Zaghib, M. Trudeau, A. Guerfi, J. Trottier, A. Mauger, R. Veillette, C.M. Julien, *J. Power Sources*, 204 (2012) 177.
22. G. Meligrana, F. Di Lupo, S. Ferrari, M. Destro, S. Bodoardo, N. Garino, C. Gerbaldi, *Electrochimica Acta*, 105 (2013) 99.
23. J. Nava-Avendaño, M.R. Palacín, J. Oró-Solé, A. Ponrouch, J.-M. Tarascon, N. Recham, *Solid State Ionics*, 263 (2014) 157.
24. Z. Dai, L. Wang, X. He, F. Ye, C. Huang, J. Li, J. Gao, J. Wang, G. Tian, M. Ouyang, *Electrochimica Acta*, 112 (2013) 144.
25. X. Li, S. Liu, H. Jin, Y. Meng, Y. Liu, *J. Alloys Comp.*, 614 (2014) 7.
26. S.-M. Oh, H.-G. Jung, C.S. Yoon, S.–T. Myung, Z. Chen, K. Amine, Y.-K. Sun, *J. Power Sources*, 196 (2011) 6924.
27. Y.-J. Zhong, J.-T. Li, Z.-G. Wu, X.-D. Guo, B.-H. Zhong, S.-G. Sun, *J. Power Sources*, 234 (2013) 217.
28. K. Kagesawa, E. Hosono, M. Okubo, D. Nishio-Hamane, T. Kudo, H. Zhou, *J. Power Sources*, 248 (2014) 615.
29. P. Zuo, G. Cheng, L. Wang, Y. Ma, C. Du, X. Cheng, Z. Wang, G. Yin, *J. Power Sources*, 243 (2013) 872.
30. H. Fang, Z. Pan, L. Li, Y. Yang, G. Yan, G. Li, S. Wei, *Electrochem. Commun.*, 10 (2008) 1071.
31. Q. Zhuang, S. Xu, X. Qiu, Y. Cui, L. Fang, S. Sun, *Progress in Chemistry* (Chinese), 22 (2010) 1044.
32. J. Kim, D.-H. Seo, S.-W. Kim, Y.-U. Park and K. Kang, *Chem. Commun.*, 46 (2010) 1305.

© 2015 The Authors. Published by ESG (www.electrochemsci.org). This article is an open access article distributed under the terms and conditions of the Creative Commons Attribution license (http://creativecommons.org/licenses/by/4.0/).